


**Nonreciprocal quantum coherence in spinning magnomechanical systems**Haoqi Zhang,<sup>1</sup> Xianxin Shang,<sup>1</sup> Qinghong Liao,<sup>2</sup> Aixi Chen,<sup>3,\*</sup> and Wenjie Nie<sup>1,†</sup><sup>1</sup>*Department of Applied Physics, East China Jiaotong University, Nanchang 330013, China*<sup>2</sup>*Department of Electronic Information Engineering, Nanchang University, Nanchang 330031, China*<sup>3</sup>*Department of Physics, Zhejiang Sci-Tech University, Hangzhou 310018, China* (Received 26 June 2023; revised 17 November 2023; accepted 22 December 2023; published 24 January 2024)

We theoretically investigate the quantum coherence and its nonreciprocity in a cavity magnomechanical system composed of a spinning microwave resonant cavity and an yttrium iron garnet sphere. The optical Fizeau shift related to the driving direction of the microwave cavity is responsible for an important source of nonreciprocity in the stability of the system, which leads to the nonreciprocal quantum coherence. Remarkably, the quantum coherence of the mechanical motion mode can be greater than that of the microwave photon and the magnon modes, which describes a significant enhancement of the correlations of the system. We also analyze in detail the influence of the strength of the magnomechanical coupling, the Kerr nonlinearity, and the effective detunings on the quantum coherence. Our paper paves the way for optimizing the stability range of coupled systems and maintaining more reliable quantum coherence by designing and modulating the system parameters in cavity magnetomechanical systems.

DOI: [10.1103/PhysRevA.109.013719](https://doi.org/10.1103/PhysRevA.109.013719)**I. INTRODUCTION**

Recently, the cavity magnomechanical system including an yttrium iron garnet (YIG) material has drawn considerable attention [1], which provides an ideal platform for studying the quantum properties of a mechanical motion mode and the nonreciprocal transmission of a microwave field [2]. Especially the YIG spheres in the system have a relatively high spin density [3–7] and low damping rate and therefore a strong light-matter interaction between the subsystems can be realized. For example, the magnon mode in the magnomechanical system can be generated by the collective spin motion of a large number of zero wave vectors (Kittel mode) in the YIG and strongly coupled to the microwave cavity photons through the magnetic dipole interactions at cryogenic or room temperature [8]. Simultaneously, the phonon mode comes from the mechanical deformation of the YIG sphere and can be coupled to the magnon mode by the magnetostrictive force [9,10]. Based on the hybrid couplings between the subsystems, some interesting quantum properties, such as the magnon squeezed states [11–13], the steady Bell state generation via magnon-photon coupling [14], and the photon-magnon-phonon tripartite entanglement state [9], are investigated in detail. In addition, the remote manipulation of spin current, magnon lasers based on Brillouin light scattering, and magnetically manipulated slow light [15,16] is explored carefully by designing the magnomechanical systems. In general, the cavity magnomechanical system has great flexibility in contrast to an optomechanical system with movable mechanical parts [17], since the frequency of the

magnon excitation can be tuned by adjusting the bias magnetic field [8,18,19]. Furthermore, the concept of the magnon Kerr effect caused by the anisotropy of magnetocrystalline in YIG crystal has been proposed and experimentally demonstrated in a strongly coupled cavity-magnon system [20,21], which brings about many intriguing phenomena, such as the magnon-induced high-order sideband generation and bistability [2,22].

It is noted that the quantum coherence is a defining feature of coupled quantum systems, which describes the significant correlation between the quantum fluctuations of the system [23–30] and can be regarded as an essential element for the quantum information processing [31–35], quantum metrology [36], exciton and electron transport in biomolecular networks [37–41], and phase transition [42,43]. Based on various macroscopic structures, i.e., the Josephson junction [44–46], a superconducting quantum circuit, and optomechanical systems [47–50], the macroscopic quantum coherence has been explored in detail. Remarkably, in order to compare the classical and quantum properties of the system, the concept of classical states must be specified to classify the resources of quantum technologies [31,51]. One way to achieve this is the introduction of the concept of quantum coherence [25]. In this regard, the quantum coherence is primarily accountable for the advantage offered by quantum tasks [32]. Physically, quantum coherence can be used as a resource to generate quantum entanglement [52–55]. This especially leads to a one-to-one transfer of single-mode nonclassical correlations to entanglement in quantum optics [56]. More importantly, as a key factor in promoting quantum technology, it is very desirable to be able to accurately quantify the usefulness of coherence as a resource for such applications. In terms of quantifying quantum coherence, many different measures of quantum coherence have been proposed, such as relative

\*aixichen@zstu.edu.cn

†niewenjiezh@ sina.cn

entropy of coherence [24], convex-roof coherence measurement [26], and geometric and concurrence measurements [27,28,30]. Quantitative description of quantum coherence helps to probe macroscopic quantum patterns through the method of optical detection [53,57,58]. Nonetheless, the quantum coherence of open systems is easily influenced by the surrounding environment and will eventually disappear with the dissipation of the surroundings. These dissipative problems require further development of quantum coherence optimization control.

Nonreciprocal elements also have attracted a great deal of interest [59–66], which are crucial in many scientific fields, such as invisible sensing or cloaking, acoustics, thermodynamics, rotating resonators, and nanophotonic communication systems [67–70]. As an important application, the design of nonreciprocal devices allows signals to propagate in one direction and prevents signals from propagating in the opposite direction, and therefore plays a key role in backaction-immune communications. Traditionally, people break the time-reversal symmetry by magneto-optical (Faraday-rotation) crystals [71,72] to realize nonreciprocity. However, such devices tend to be bulky, costly, and unsuitable for on-chip integration. Hence, it is of great interest to pursue alternative mechanisms to break the reciprocity of light on a microscale platform. Over the past few years, nonreciprocal devices including circulators [73,74], isolators or diodes [75–77], and directional amplifiers [78] have been proposed theoretically and implemented experimentally [79,80]. In addition, an optical diode with 99.6% isolation has been experimentally demonstrated using a spinning resonator, where the nonreciprocity is caused by the Fizeau shift of circulating lights [81]. Further, the Fizeau shift of circulating lights in spinning microwave magnomechanical or cavity optomechanical systems can be designed to realize the nonreciprocal transmission and the nonreciprocal quantum entanglement of light and motion [82–84].

The context of this paper highlights a proposed rotating microwave magnomechanical system, which is composed of a microwave cavity and an embedded YIG sphere with a magnon and a mechanical mode. We also noticed that in a recent study of a rotating microwave resonator, Zheng *et al.* [84] have demonstrated how the Fizeau shift in a cavity magnonic system induces the nonreciprocal tripartite entanglement among the microwave photon and two magnon modes. In contrast, we aim to make the circulating light in the resonant cavity undergo Fizeau shift by adjusting different driving directions, ultimately leading to different effective detunings of the photons and generating nonreciprocity of the quantum coherence of a target mode, i.e., photon, magnon, or phonon mode. To this end, we focused on the quantification of coherence in bosonic Gaussian states of infinite-dimensional systems, which is evaluated by the coherence measurement based on the relative entropy [24]. We found that the Fizeau shift of the microwave resonator leads to a significant difference in the system stability and the quantum coherence for driving the cavity field from opposite directions. In parallel, considering the feasible parameters in the experiment, we show the influence of the driving power of the cavity field, the magnomechanical and magnon-photon couplings, the Kerr coefficient, and the effective detuning of the cavity photon

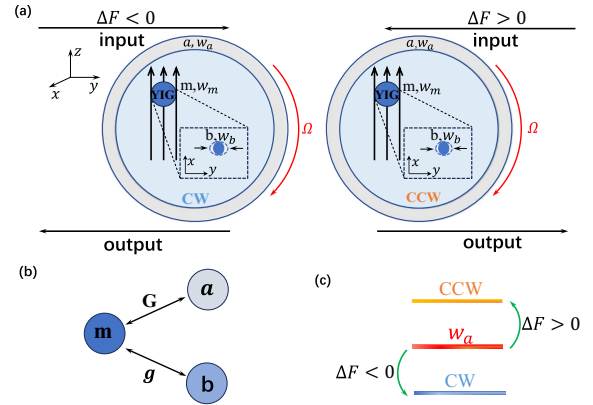


FIG. 1. (a) Sketch of the system. A YIG sphere is placed inside a microwave cavity near the maximum magnetic field of the cavity mode and biased by a uniform magnetic field along the  $z$  direction. (b) Equivalent schematic diagram of the hybrid coupled system, where  $G$  and  $g$  are the coupling strengths of the magnon mode to the cavity mode and the mechanical mode, respectively. (c) Changes in microwave frequency. When the microwave resonator rotates in the fixed clockwise (CW) direction, the resonance frequencies of the CW and the counterclockwise (CCW) photon modes will experience different Fizeau shifts. The Fizeau shift  $\Delta F < 0$  corresponds to the situation of driving the microwave resonator from the left ( $y$  axis) side, while  $\Delta F > 0$  means that the microwave resonator is driven from the right ( $-y$  axis) side.

and magnon mode on the quantum coherence. In particular, by properly selecting the parameters and stable region of the system, the quantum coherence of the mechanical motion can be greater than that of the microwave photon and magnon mode, which can be seen as the result of the quantum coherence transfer from the photon and magnon modes to the mechanical mode. These results open a door toward the synthesis of novel microscale magnon structures for potential applications in realizing highly tunable information processing and quantum communications.

The paper is organized as follows. In Sec. II, we give the theoretical model and derive the Heisenberg-Langevin equation describing the system dynamics. In Sec. III, we quantify the quantum coherence of the target modes in the system and analyze the influence of the external parameters on the quantum coherence in detail. Finally, a short summary of the paper is given in Sec. IV.

## II. SYSTEM MODEL AND DYNAMICS

The three-mode coupled cavity magnomechanical system, as schematically shown in Figs. 1(a) and 1(b), consists of a spinning microwave resonator and a YIG sphere in which the magnon mode described by collective motions of a number of spins is coupled to the deformation (phonon) mode of the sphere. Moreover, the magnon mode can be coupled significantly to the microwave mode via the magnetic-dipole interaction when the YIG sphere is placed close to the maximum magnetic field of the microwave cavity, which is driven by an external laser field with power  $P$ . We also assume that

the Kerr nonlinear effect originated from the magnon-magnon scattering is included to comprehensively influence the characteristics of the system. The total Hamiltonian of the system reads (setting  $\hbar = 1$ ) [9,68]

$$H = (\omega_a + \Delta F)\hat{a}^\dagger\hat{a} + \omega_m\hat{m}^\dagger\hat{m} + \omega_b\hat{b}^\dagger\hat{b} + g\hat{m}^\dagger\hat{m}(\hat{b}^\dagger + \hat{b}) + G(\hat{m}^\dagger\hat{a} + \hat{a}^\dagger\hat{m}) + K\hat{m}^\dagger\hat{m}\hat{m}^\dagger\hat{m} + i\varepsilon(\hat{a}^\dagger e^{-i\omega_d t} - \hat{a}e^{i\omega_d t}), \quad (1)$$

where  $\hat{a}^\dagger(\hat{a})$ ,  $\hat{b}^\dagger(\hat{b})$ , and  $\hat{m}^\dagger(\hat{m})$  are the bosonic creation (annihilation) operators of the cavity mode, the phonon mode, and the magnon mode, respectively.  $\omega_a$ ,  $\omega_b$ , and  $\omega_m$  are the resonance frequencies corresponding to the target modes  $a$ ,  $b$ , and  $m$ . By spinning the microwave resonator, the resonance frequency of the photon mode undergoes a Fizeau shift that depends on the amplitude and direction of the angular velocity of the spinning cavity [68,81,85], i.e.,  $\omega_a \rightarrow \omega_a + \Delta F$  with  $\Delta F = \pm \frac{nr\Omega\omega_a}{c}(1 - \frac{1}{n^2} - \frac{\lambda}{n} \frac{dn}{d\lambda})$ . Here  $r(n)$  is the radius (refractive index) of the microwave resonator, and  $c$  ( $\lambda$ ) is the speed (wavelength) of microwave photons in vacuum. In Fig. 1(c), we describe the changes in microwave frequency due to the rotation. That is, when the microwave resonator rotates in the fixed clockwise direction, the Fizeau shift  $\Delta F < 0$  ( $\Delta F > 0$ ) corresponds to the situation of driving the microwave resonator from its left (right) side [82]. In the case of the Fizeau shift due to the rotation, the opposite frequency shift of these two backpropagation modes will result in the steady states of the system being related to the direction of microwave propagation, thereby disrupting the system's time-reversal symmetry and inducing the generation of various nonreciprocities in the system. In addition, the magnon frequency in the YIG sphere is proportional to the external bias magnetic field  $H_0$ , i.e.,  $\omega_m = \gamma H_0$  with  $\gamma/2\pi = 28\text{GHz/T}$  being the gyromagnetic ratio [9]. In contrast, the frequency of the phonon mode in the YIG sphere generally decreases with the increase of the sphere size, which has been evaluated experimentally [8]. Further, the role of the mechanical mode in the hybrid system can be inferred by sending weak probe signals into the spinning cavity and measuring its reflection. The  $G$  and  $g$  in Eq. (1) are the linear photon-magnon coupling strength and the general magnomechanical coupling strength, respectively. In the magnomechanical system, the electromagnetical coupling  $G$  can be larger than the damping rate of the microwave mode  $\kappa_a$  and of the magnon mode  $\kappa_m$  [86]. The Kerr nonlinear strength is symbolized by  $K$ , which is the order of magnitude of  $\mu\text{Hz}$ . The strength of the pump laser is  $\varepsilon = \sqrt{2P\kappa_a/\hbar\omega_d}$  with a driving frequency  $\omega_d$ .

In a rotating frame with the cavity driving frequency  $\omega_d$ , the Hamiltonian (1) of the three-mode system can be written as

$$H = (\Delta_a + \Delta F)\hat{a}^\dagger\hat{a} + \Delta_{m0}\hat{m}^\dagger\hat{m} + \omega_b\hat{b}^\dagger\hat{b} + g\hat{m}^\dagger\hat{m}(\hat{b}^\dagger + \hat{b}) + K\hat{m}^\dagger\hat{m}\hat{m}^\dagger\hat{m} + G(\hat{m}^\dagger\hat{a} + \hat{a}^\dagger\hat{m}) + i\varepsilon(\hat{a}^\dagger - \hat{a}), \quad (2)$$

where  $\Delta_a = \omega_a - \omega_d$  ( $\Delta_{m0} = \omega_m - \omega_d$ ) is the detuning between the photon (magnon) mode and the driving field. In terms of Eq. (2), it can be easily concluded that the dynamics of the system are reciprocal and will be independent of the driving direction of the pump field when the microwave cavity

is stationary and therefore there is no contribution of Fizeau shift in the effective cavity detuning  $\Delta_a + \Delta F$ . Conversely, when the microwave cavity rotates, the effective cavity detuning  $\Delta_a + \Delta F$  increases or decreases because the different driving direction of the system will lead to opposite Fizeau shifts. Consequently, an increase or decrease in the effective detuning will cause the system to operate in different steady states, which significantly affects the quantum fluctuation dynamics of the system and alters the characteristics of quantum coherence in the system. In particular, for the same angular velocity, due to the opposite frequency shift for the forward and backward drive, the quantum coherence may appear unidirectionally. It is worth noting that the realization of asymmetric quantum properties can be achieved by simply increasing or decreasing the cavity detuning  $\Delta_a$  even in the absence of the Fizeau shift. However, the realization of these quantum coherence properties requires us to choose different driving frequencies  $\omega_d$ , which is actually the result of changing the parameter characteristics of the system. Here, our main purpose is to study the generation of nonreciprocal quantum coherence in a cavity magnomechanical system by controlling the driving direction of the system to achieve the opposite Fizeau shift [83].

Considering the fluctuation-dissipation processes affecting the microwave photons, phonons, and magnons in the system, the Heisenberg-Langevin equation describing the dynamics of the system are given by

$$\begin{aligned} \dot{\hat{a}} &= -[i(\Delta_a + \Delta F) + \kappa_a]\hat{a} - iG\hat{m} + \varepsilon + \sqrt{2\kappa_a}\hat{a}^{\text{in}}, \\ \dot{\hat{b}} &= -(i\omega_b + \kappa_b)\hat{b} - ig\hat{m}^\dagger\hat{m} + \sqrt{2\kappa_b}\hat{b}^{\text{in}}, \\ \dot{\hat{m}} &= -(i\Delta_{m0} + \kappa_m)\hat{m} - iG\hat{a} - ig\hat{m}(\hat{b}^\dagger + \hat{b}) \\ &\quad - iK\hat{m} - 2iK\hat{m}^\dagger\hat{m}\hat{m} + \sqrt{2\kappa_m}\hat{m}^{\text{in}}, \end{aligned} \quad (3)$$

where  $\kappa_b$  stands for the decay rate of the phonon mode. The  $\hat{\delta}^{\text{in}}(o = a, b, m)$  describes the input noise operators of the target mode  $o$ , which has a zero mean value and is fully characterized by the following correlation functions:  $\langle \hat{\delta}^{\text{in}\dagger}(t)\hat{\delta}^{\text{in}}(t') \rangle = N_o\delta(t - t')$  and  $\langle \hat{\delta}^{\text{in}}(t)\hat{\delta}^{\text{in}\dagger}(t') \rangle = (N_o + 1)\delta(t - t')$  with  $N_o = [\exp(\hbar\omega_o/k_B T) - 1]^{-1}$  being the mean thermal phonon number. Here  $k_B$  denotes the Boltzmann constant and  $T$  is the environmental temperature of the whole system.

Next we derive the linearized dynamics of the quantum fluctuations around the steady-state expectation values of the coupled system. This requires the system to be driven by a strongly pumped laser, so that the operators in Eq. (3) can be decomposed as the sum of the steady-state value and a small fluctuation, i.e.,  $\hat{o} = \langle o \rangle + \delta\hat{o}$ . By inserting this expansion into Eq. (3), the time evolution equations for the steady-state values can be obtained as

$$\begin{aligned} 0 &= -[i(\Delta_a + \Delta F) + \kappa_a]\langle a \rangle - iG\langle m \rangle + \varepsilon, \\ 0 &= -(i\omega_b + \kappa_b)\langle b \rangle - ig|\langle m \rangle|^2, \\ 0 &= -(i\Delta_{m0} + \kappa_m)\langle m \rangle - iG\langle a \rangle - iK\langle m \rangle \\ &\quad - ig\langle m \rangle(\langle b \rangle + \langle b \rangle^\dagger) - 2iK|\langle m \rangle|^2\langle m \rangle. \end{aligned} \quad (4)$$

In terms of Eq. (4), the steady-state solutions of the dynamical variables are as follows:

$$\begin{aligned} (a) &= \frac{-iG\langle m \rangle + \varepsilon}{i\Delta'_a + \kappa_a}, \\ (b) &= \frac{-ig|\langle m \rangle|^2}{i\omega_b + \kappa_b}, \\ \langle m \rangle &= \frac{-iG\varepsilon}{(i\Delta_m + \kappa_m)(i\Delta'_a + \kappa_a) + G^2}, \end{aligned} \quad (5)$$

where  $\Delta'_a = \Delta_a + \Delta F$ , and  $\Delta_m = \Delta_{m0} + g(\langle b \rangle + \langle b \rangle^\dagger) + 4K|\langle m \rangle|^2$  are the effective detunings of the cavity and magnon modes. We further introduce the quadrature fluctuation operators defined as  $\delta X_o = (\delta\hat{o} + \delta\hat{o}^\dagger)/\sqrt{2}$  and  $\delta Y_o = (\delta\hat{o} - \delta\hat{o}^\dagger)/(\sqrt{2}i)$ , and the corresponding noise operators defined as  $X_o^{\text{in}} = (\delta\hat{o}^{\text{in}} + \delta\hat{o}^{\text{in}\dagger})/\sqrt{2}$  and  $Y_o^{\text{in}} = (\delta\hat{o}^{\text{in}} - \delta\hat{o}^{\text{in}\dagger})/(\sqrt{2}i)$ . Then the linearized quantum Langevin equations are calculated as

$$\begin{aligned} \delta\dot{X}_a &= \Delta'_a\delta Y_a + G\delta Y_m - \kappa_a\delta X_a + \sqrt{2\kappa_a}X_a^{\text{in}}(t), \\ \delta\dot{Y}_a &= -\Delta'_a\delta X_a - G\delta X_m - \kappa_a\delta Y_a + \sqrt{2\kappa_a}Y_a^{\text{in}}(t), \\ \delta\dot{X}_b &= w_b\delta Y_b - \kappa_b\delta X_b + \sqrt{2\kappa_b}X_b^{\text{in}}(t), \\ \delta\dot{Y}_b &= -w_b\delta X_b - \kappa_b\delta Y_b - g(\langle m \rangle + \langle m \rangle^*)\delta X_m \\ &\quad + ig(\langle m \rangle - \langle m \rangle^*)\delta Y_m + \sqrt{2\kappa_b}Y_b^{\text{in}}(t), \\ \delta\dot{X}_m &= ig(\langle m \rangle^* - \langle m \rangle)\delta X_b + G\delta Y_a - \kappa_m\delta X_m \\ &\quad + (\Delta_m - 2K|\langle m \rangle|^2)\delta Y_m + \sqrt{2\kappa_m}X_m^{\text{in}}(t), \\ \delta\dot{Y}_m &= -\kappa_m\delta Y_m - G\delta X_a - g(\langle m \rangle + \langle m \rangle^*)\delta X_b \\ &\quad - (\Delta_m + 2K|\langle m \rangle|^2)\delta X_m + \sqrt{2\kappa_m}Y_m^{\text{in}}(t). \end{aligned} \quad (6)$$

Here we consider that the system starts from Gaussian states. In this case, the system dynamics governed by the linearized Eq. (6) evolves always in Gaussian and the state of the system is completely determined by the  $6 \times 6$  correlation matrix with matrix element  $V_{ij} = \langle u_i(t)u_j(t) + u_j(t)u_i(t) \rangle / 2$  [87], where  $u(t) = [\delta X_a(t), \delta Y_a(t), \delta X_b(t), \delta Y_b(t), \delta X_m(t), \delta Y_m(t)]^T$  is the vector of the fluctuation operator. In the steady state, the correlation matrix of the system satisfies the following Lyapunov equation [53]:

$$AV + VA^T = -D, \quad (7)$$

where  $D = \text{diag}[(2N_a + 1)\kappa_a, (2N_a + 1)\kappa_a, (2N_b + 1)\kappa_b, (2N_b + 1)\kappa_b, (2N_m + 1)\kappa_m, (2N_m + 1)\kappa_m]$  is the noise matrix and  $A$  is the coefficient matrix of Eq. (6),

$$A = \begin{bmatrix} -\kappa_a & \Delta'_a & 0 & 0 & 0 & G \\ -\Delta'_a & -\kappa_a & 0 & 0 & -G & 0 \\ 0 & 0 & -\kappa_b & \omega_b & 0 & 0 \\ 0 & 0 & -\omega_b & -\kappa_b & g_1 & g_2 \\ 0 & G & -g_2 & 0 & -\kappa_m & \Delta'_m \\ -G & 0 & g_1 & 0 & -\Delta''_m & -\kappa_m \end{bmatrix}, \quad (8)$$

where  $g_1 = -g(\langle m \rangle + \langle m \rangle^*)$ ,  $g_2 = ig(\langle m \rangle - \langle m \rangle^*)$ ,  $\Delta''_m = \Delta_m + 2K|\langle m \rangle|^2$ , and  $\Delta'_m = \Delta_m - 2K|\langle m \rangle|^2$ .

We are interested in the generation of macroscopic quantum properties in a cavity magnomechanical system which

can be explored by solving the correlation matrix in Eq. (8). To this end, the coupled system must reach a unique steady state conforming to the Routh-Hurwitz criterion, which can be achieved by selecting appropriate external system parameters to ensure that all eigenvalues of the matrix  $A$  have negative real part, i.e.,  $E_{\text{max}} = \max\{\text{Real}[\text{Eig}(A)]\} < 0$ . However, in the present model we will not list the analytical conditions due to its complicated expressions but instead check the stability of the system through numerical calculations.

### III. NONRECIPROCAL QUANTUM COHERENCE

We first evaluate the quantum coherence of the target modes in the coupled system. Physically, quantum coherence describes the degree of correlation between quantum fluctuations of the quadrature operators in the system [23–30] and is necessary for generating entanglement [88]. For the present continuous-variable system, we adopt the relative entropy in terms of the Gaussian state to quantify the quantum coherence, which is determined by the first and second moments of the Gaussian state [24,31]. For example, for a given one-mode Gaussian state  $\rho(\mathbf{V}_o, \vec{d}_o)$  with the fluctuation quadratures  $\delta X_o$  and  $\delta Y_o$ , its first moment is the mean value of the quadrature vector, i.e.,  $\vec{d}_o = (d_{o1}, d_{o2})$  with  $d_{o1} = (\langle o \rangle + \langle o \rangle^*)/\sqrt{2}$  and  $d_{o2} = (\langle o \rangle - \langle o \rangle^*)/i\sqrt{2}$ , while the second moment  $\mathbf{V}_o$  is the covariance matrix extracted from the correlation matrix  $V$  in Eq. (7). That is, the second moments of the photon mode, the photon mode, and the magnon mode in the system are, respectively,

$$\begin{aligned} \mathbf{V}_a &= \begin{pmatrix} V_{11} & V_{12} \\ V_{21} & V_{22} \end{pmatrix}, \\ \mathbf{V}_b &= \begin{pmatrix} V_{33} & V_{34} \\ V_{43} & V_{44} \end{pmatrix}, \\ \mathbf{V}_m &= \begin{pmatrix} V_{55} & V_{56} \\ V_{65} & V_{66} \end{pmatrix}. \end{aligned}$$

Then, the quantum coherence of photon mode, magnon mode, and phonon mode can be witnessed when [24]

$$C_o[\rho(\mathbf{V}_o, \vec{d}_o)] = -F(v_o) + F(2\bar{n}_o + 1) > 0, \quad (9)$$

where the specific expression of the function  $F$  is  $F(X) = \frac{X+1}{2}\log_2(\frac{X+1}{2}) - \frac{X-1}{2}\log_2(\frac{X-1}{2})$ .  $v_o = \sqrt{\text{Det}(\mathbf{V}_o)}$  is the symplectic eigenvalue of the target mode  $o$  and  $\bar{n}_o = [\text{Tr}(\mathbf{V}_o) + d_{o1}^2 + d_{o2}^2 - 2]/4$  is determined by the first and second moments of the target mode  $o$ . Finally, according to the definition in Eq. (9), the quantum coherence corresponding to the target mode  $a$ ,  $b$ , and  $m$  can be expressed as [24]

$$\begin{aligned} C_a &= C_a[\rho(\mathbf{V}_a, \vec{d}_a)], \\ C_b &= C_b[\rho(\mathbf{V}_b, \vec{d}_b)], \\ C_m &= C_m[\rho(\mathbf{V}_m, \vec{d}_m)]. \end{aligned} \quad (10)$$

We stress that the quantum coherence  $C_a$ ,  $C_b$ , or  $C_m$  of the one-mode Gaussian state can be evaluated experimentally, as the first and second moments of each target mode can be acquired straightforwardly or indirectly through homodyne detection of the output field [53]. Moreover, the present methods are based on the mean-field approximation around the

steady-state expectation values in Eq. (5). Therefore, these results change explicitly if one goes beyond this approximation. This is because the performance parameters describing quantum properties, such as quantum coherence  $C_a$ ,  $C_b$ , and  $C_m$ , fail when the system works beyond the linearized picture. In essence, this is the result that the steady state of the quantum fluctuations in the system cannot be fully characterized by a  $6 \times 6$  correlation matrix  $V$ . The evaluation of the quantum properties (such as coherence) for a non-Gaussian state induced by the hybrid couplings requires knowledge about the third- and fourth-order cumulants in the system in addition to the first and second cumulants (moments) [89,90]. In the present paper, in order to ensure that the system works in the linearization regime, the driving power selected is always large enough.

In the following, we numerically evaluate the nonreciprocal characteristics of the quantum coherence induced by the rotation of the microwave cavity. Furthermore, we also study what kind of parameter range can be used to realize that the quantum coherence of the macroscopic phonon mode exceeds that of the other two modes. We select the accessible parameters of the microwave cavity, i.e., the frequency of the driving field,  $\omega_d = 2\pi \times 10.1 \times 10^9$  Hz [2,86], and the decay rate of the microwave cavity  $\kappa_a = 2\pi \times 2 \times 10^6$  Hz. The frequency and the dissipation rate of the mechanical YIG sphere are  $\omega_b = 2\pi \times 10 \times 10^6$  Hz and  $\kappa_b = 2\pi \times 100$  Hz, respectively. The effective detuning of the magnon mode and the decay rate of the magnon mode are  $\Delta_m = 0.1\omega_b$  and  $\kappa_m = 2\pi \times 0.56 \times 10^6$  Hz, respectively. We also assume that the magnon and photon modes are in resonance, that is,  $\Delta_a = \omega_b$ . The strengths of the photon-magnon and phonon-magnon couplings are  $G = 2\pi \times 10 \times 10^5$  Hz and  $g = 2\pi \times 1$  Hz, respectively. The Kerr nonlinearity  $K = 2\pi \times 0.2 \times 10^{-6}$  Hz and the temperature of the system is  $T = 1.5$  K.

Figure 2 shows the quantum coherence of the photon, phonon, and magnon modes  $C_a$ ,  $C_b$ , and  $C_m$ , as a function of the nondimensionalized driving power  $P/P_0$  with  $P_0 = 1.007$  nW being the driving power corresponding to a natural energy scale of the driving strength  $\varepsilon = \omega_d$ . From Fig. 2, it is found that different driving directions (the left or right) will result in different quantum coherence  $C_a$ ,  $C_b$ , and  $C_m$ . For example, compared with the stationary case with  $\Delta F = 0$ , the quantum coherences  $C_a$ ,  $C_b$ , and  $C_m$  of the spinning magnomechanical system always increase for  $\Delta F < 0$ , while they decrease for  $\Delta F > 0$ . In addition, the power range generating quantum coherence narrows when  $\Delta F < 0$ , and widens when  $\Delta F > 0$ . This is because the generation of quantum coherence is always limited by the stability of the system. When the rotation of the magnetomechanical system is considered, the stability of the system is nonreciprocal with different driving directions, which leads to the nonreciprocal quantum coherence. Moreover, we find that the quantum coherences of the photon and the magnon modes are always larger than that of the mechanical mode, i.e.,  $C_a > C_b$  and  $C_m > C_b$ . This results from the fact that the environmental incoherence of the mechanical mode is usually greater than that of the microwave field and magnon mode. We emphasize that the quantum coherence of the phonon mode  $C_b$  is significantly related to the dissipation rate  $\kappa_b$  of the phonon mode, which determines the degree of environmental incoherence of the mechanical mode.

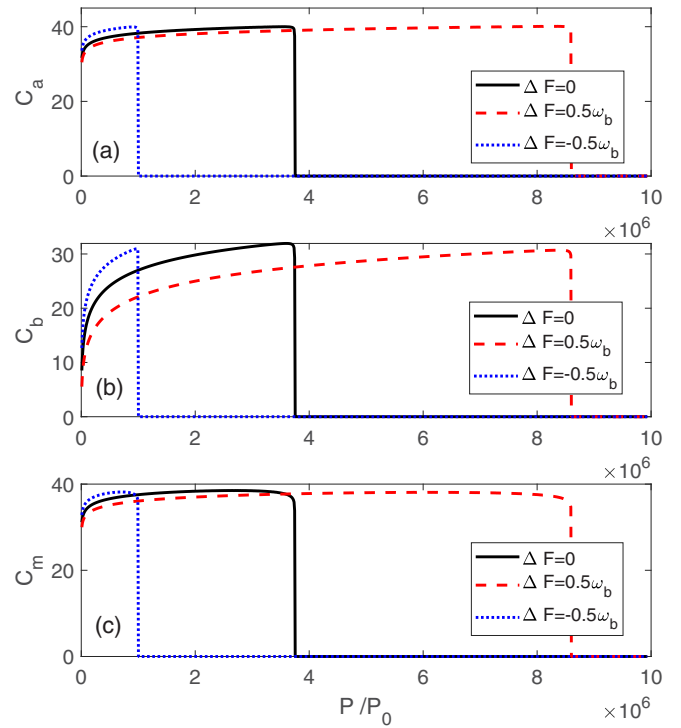


FIG. 2. Quantum coherences  $C_a$  (a),  $C_b$  (b), and  $C_m$  (c), as functions of the nondimensionalized driving power  $P/P_0$  with three different scenarios  $\Delta F = 0, 0.5\omega_b$ , and  $-0.5\omega_b$ . The other parameter values are  $\omega_d = 2\pi \times 10.1 \times 10^9$  Hz,  $\omega_b = 2\pi \times 10 \times 10^6$  Hz,  $\kappa_b = 2\pi \times 100$  Hz,  $\kappa_a = 2\pi \times 2 \times 10^6$  Hz,  $\kappa_m = 2\pi \times 0.56 \times 10^6$  Hz,  $G = 2\pi \times 10 \times 10^5$  Hz,  $g = 2\pi \times 1$  Hz,  $K = 2\pi \times 0.2 \times 10^{-6}$  Hz,  $\Delta_m = 0.1\omega_b$ ,  $\Delta_a = \omega_b$ ,  $P_0 = 1.007$  nW, and  $T = 1.5$  K.

In Fig. 3 we show the quantum coherence of the phonon mode  $C_b$ , as a function of the nondimensionalized driving power  $P/P_0$  with different  $\kappa_b$  at given  $\Delta F = 0.5\omega_b$ . From Fig. 3, it can be clearly seen that the quantum coherence  $C_b$  increases with the decrease of the dissipation rate  $\kappa_b$ . As a result, a smaller decay rate  $\kappa_b$  is the preferred choice for enhancing the quantum coherence of the mechanical mode. In order to show

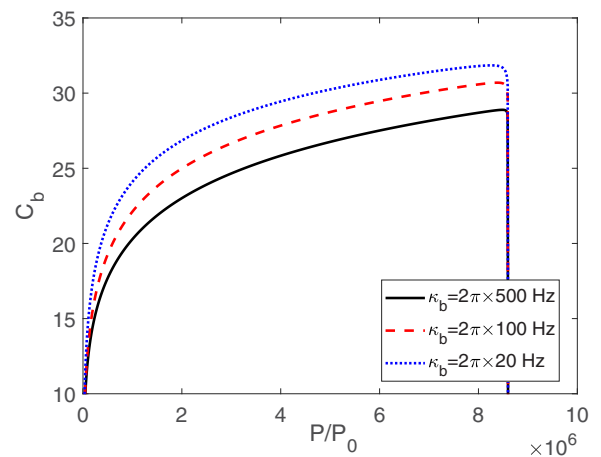


FIG. 3. Quantum coherence  $C_b$  as functions of the nondimensionalized driving power  $P/P_0$  with different  $\kappa_b$  at given  $\Delta F = 0.5\omega_b$ . The other parameter values are the same as those in Fig. 2.

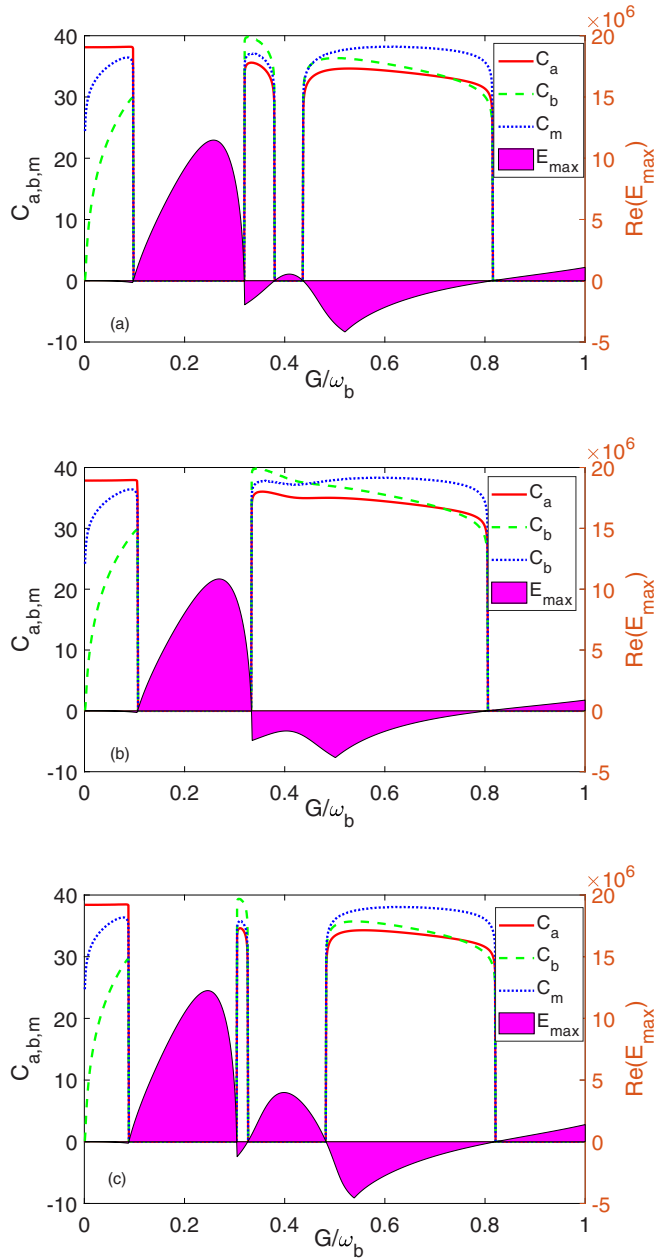


FIG. 4. Quantum coherences  $C_a$ ,  $C_b$ , and  $C_m$  and the real part of the maximum eigenvalue  $E_{\max}$  as a function of the ratio  $G/\omega_b$  with three different scenarios  $\Delta F = 0$  (a),  $\Delta F = 0.1\omega_b$  (b), and  $\Delta F = -0.1\omega_b$  (c). The pink area surrounded by black lines of eigenvalues  $E_{\max}$  depicts the stability of the system. Here the driving laser power is  $P = 9.931 \times 10^5 P_0$ , the magnomechanical coupling is  $g = 2\pi \times 2$  Hz, and the other parameter values are the same as those in Fig. 2.

the generation of quantum coherence and its nonreciprocity in the stability region more clearly, in Fig. 4, we depicted the quantum coherences  $C_a$ ,  $C_b$ , and  $C_m$  and the maximum eigenvalue of the matrix  $A$  as a function of the magnon-photon coupling strength  $G$  with different  $\Delta F$  at the pump power  $P = 9.931 \times 10^5 P_0$  and the magnomechanical coupling  $g = 2\pi \times 2$  Hz. It is found that the stability of the coupled system depends strongly on the coupling strength  $G$  and the Fizeau shift  $\Delta F$ . Compared with the stationary case with

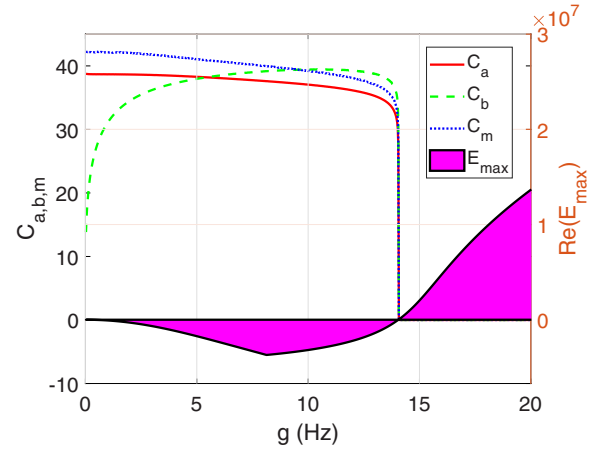


FIG. 5. Quantum coherences  $C_a$ ,  $C_b$ , and  $C_m$  and the real part of the maximum eigenvalue  $E_{\max}$  as the function of the magnon-phonon coupling  $g$ . The driving laser power is  $P = 4.965 \times 10^6 P_0$ ,  $\Delta F = 0.1\omega_b$ , and the other parameters are the same as those in Fig. 2.

$\Delta F = 0$ , the range of the  $G$  with positive eigenvalue value narrows when  $\Delta F < 0$ , and widens when  $\Delta F > 0$ . Therefore, the quantum coherence of the system will be nonreciprocal and can be established within a relatively large coupling range of  $G$  for  $\Delta F > 0$ . Further, from Fig. 4 we can see clearly that the quantum coherence of a single mode, i.e.,  $C_a$ ,  $C_b$ , or  $C_m$ , is not a monotonic function of the ratio  $G/\omega_b$  and always vanishes when the system works in the unstable regime with the positive eigenvalues. In particular, the values of  $C_a$ ,  $C_b$ , and  $C_m$  decrease rapidly to zero at each stable-unstable critical point so that the quantum coherences of the system change significantly. Another interesting feature is that when the system operates in a stable region with moderate coupling strength  $G$ , the quantum coherence of the phonon mode is always greater than that of the photon and the magnon modes, i.e.,  $C_b > C_{a,m}$ . For example, in the absence of the Fizeau shift  $\Delta F$ , the range of the coupling strength  $G$  corresponding to the inverted quantum coherence (i.e.,  $C_b > C_{a,m}$ ) is between  $0.319\omega_b$  and  $0.380\omega_b$ . The range of the  $G$  with inverted quantum coherence will be widened when  $\Delta F > 0$ , i.e.,  $0.333\omega_b < G < 0.447\omega_b$ . Conversely, the range of the  $G$  reduces to  $0.304\omega_b < G < 0.327\omega_b$  when  $\Delta F < 0$ . These inverted characteristics mean that the coupling between the subsystems can resist the environmental incoherence of the mechanical mode and induce a significant enhancement of the correlations of the system. When the coupling strength  $G$  becomes relatively large, such as  $G = 0.5\omega_b$ , the quantum coherence of the phonon mode is greater than that of the photon mode, but less than that of the magnon mode, i.e.,  $C_b > C_a$  and  $C_b < C_m$ . In contrast, in the two stable regions where the coupling strength  $G$  approaches the leftmost critical point and the rightmost critical point, the phonon mode has the smallest quantum coherence. These results show that people can flexibly manipulate the quantum coherence of photon, phonon, and magnon modes and their nonreciprocal characteristics by adjusting the magnon-photon coupling strength  $G$ .

The magnomechanical coupling  $g$  between the phonons and magnons provides a direct channel for the coherence

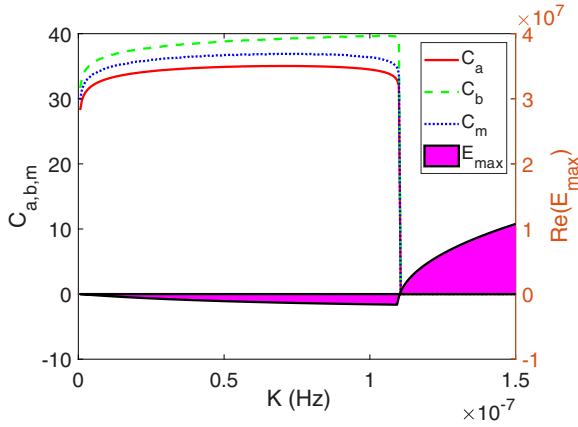


FIG. 6. Quantum coherences  $C_a$ ,  $C_b$ , and  $C_m$  and the real part of the maximum eigenvalue  $E_{\max}$  as a function of the Kerr nonlinearity  $K$ . The driving laser power is  $P = 4.965 \times 10^6 P_0$ ,  $\Delta F = 0$ ,  $G = 0.38\omega_b$ , and the other parameters are the same as those in Fig. 2.

transfer between the phonon mode and the magnon mode. In Fig. 5, we depicted the quantum coherences  $C_a$ ,  $C_b$ , and  $C_m$  as a function of the magnon-phonon coupling  $g$ . Here and in the subsequent numerical simulations, we only consider the case where the microwave field is driven from the left side, i.e.,  $\Delta F = 0.1\omega_b$ . From Fig. 5, we can see clearly that the quantum coherences  $C_a$  and  $C_m$  decrease monotonously with the increase of the coupling coefficient  $g$ . In contrast, the quantum coherence of the phonon mode  $C_b$  is not a monotonous function of the coupling coefficient  $g$  and the peak appears at the intermediate value of the  $g$ , i.e.,  $g \approx 10$  Hz. That is, the degree of coherence increases first and then decreases rapidly with the increase of the coupling coefficient  $g$ . Further, when the coupling coefficient  $g$  approaches the stable-unstable critical point, i.e.,  $g = 14.07$  Hz, each single-mode quantum coherence always drops sharply to zero. This is because when the coupled system passes through the stable and unstable point and enters the unstable region, the quantum fluctuations of the system are significantly amplified, resulting in the loss of all quantum coherence in the system. Similarly, the quantum coherence of the macroscopic phonon mode can exceed simultaneously that of the other two modes, i.e.,  $C_b > C_{a,m}$ , by adjusting properly the magnon-phonon coupling  $g$ , such as  $g > 10$  Hz. These results also show that quantum coherence can be transferred from the photon and the magnon modes to the mechanical mode, which results from the direct coupling between the phonon and the magnon modes and the indirect effective beam-splitter interaction between the photon and the phonon modes.

Apart from the magnon-photon coupling, the magnon-phonon coupling, and the driving power, the quantum coherences in the system  $C_a$ ,  $C_b$ , and  $C_m$  are also related to the Kerr nonlinearity originating from the magnetocrystalline anisotropy. In Fig. 6, we depict the quantum coherences  $C_a$ ,  $C_b$ , and  $C_m$  and the maximum eigenvalue as functions of the Kerr coefficient  $K$ . We can see from Fig. 6 that the quantum coherences  $C_a$ ,  $C_b$ , and  $C_m$  increase first and then decrease with the increase of the Kerr coefficient. Furthermore, the peak of the quantum coherence  $C_b$  appears near the stable-

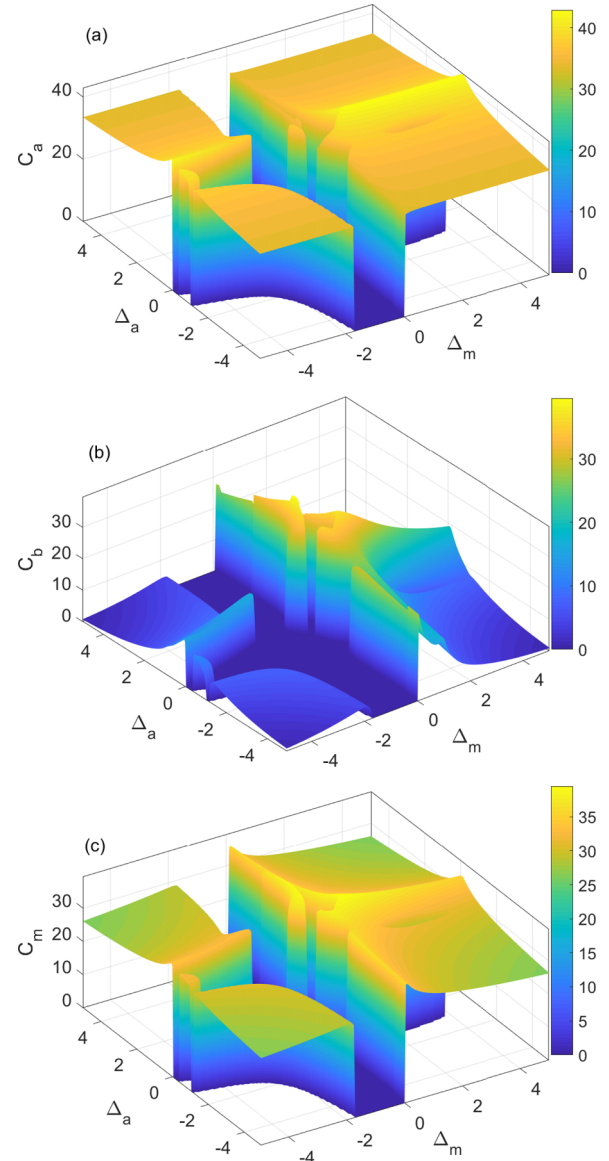


FIG. 7. Quantum coherences  $C_a$  (a),  $C_b$  (b), and  $C_m$  (c) as a function of the effective detunings  $\Delta_a$  and  $\Delta_m$ . The driving laser power is  $P = 4.965 \times 10^6 P_0$ ,  $\Delta F = 0.1\omega_b$ ,  $G = 0.38\omega_b$ , and the other parameters are the same as those in Fig. 2.

unstable critical point of the Kerr coefficient. In addition, under the selected parameters, the quantum coherence of the phonon mode is always greater than the quantum coherence of the photon mode and magnon mode. Therefore, we can select an appropriate value of the Kerr coefficient to increase the quantum coherence of the phonon mode.

We can investigate in detail the effect of the detunings of the microwave mode and magnon mode,  $\Delta_a$  and  $\Delta_m$ , on the single-mode quantum coherences  $C_a$ ,  $C_b$ , and  $C_m$ . In Fig. 7, We depict the quantum coherences  $C_a$ ,  $C_b$ , and  $C_m$  as functions of the effective detunings  $\Delta_a$  and  $\Delta_m$ . It is found from Fig. 7 that as long as the system works in the stability region, the quantum coherence of photon, phonon, and magnon modes can always be generated. As a result, we can carefully design and adjust the system parameters, such as the detunings  $\Delta_a$  and

$\Delta_m$ , to make the stability range of the coupled system as large as possible, so that we can achieve the quantum coherence in a larger parameter range. It is also noted that the stability of the coupled system depends strongly on the photon-magnon and phonon-magnon interactions, the pump power, and the Kerr coefficient in the coupled system. Further, from Figs. 7(a)–7(c), we can see clearly that the optimal values of the quantum coherence appear at the region of  $\Delta_a > 0$  and  $\Delta_m > 0$ , which results from the effective magnomechanical coupling between the subsystems.

#### IV. CONCLUSIONS

In conclusion, we have theoretically demonstrated the quantum coherence of the photon, phonon, and magnon modes in a three-mode coupled cavity magnomechanical system consisting of a microwave cavity and a YIG sphere, where the magnon mode and deformation (phonon) mode of YIG are coupled with each other by the magnetostrictive interaction when YIG is driven directly by a uniform external magnetic field. In contrast, the magnon mode and the microwave cavity mode are coupled through the magnetic dipole interaction. Our investigation shows that the optical Fizeau shift in the spinning magnomechanical system directly causes the nonreciprocal quantum coherence of the photon, phonon, and magnon modes. Further, the rotation of the microwave res-

onator leads to a significant difference in the system stability for driving the cavity field from opposite directions, which promotes the nonreciprocal characteristics of the quantum coherence of the subsystem. In particular, the quantum coherence of the mechanical motion mode can be greater than that of the microwave photon and the magnon modes when the system operates in an appropriate stable region. We stress that the quantum coherence can be transferred from the photon and the magnon modes to the mechanical mode, which is attributed to the indirect effective beam-splitter interaction between the phonon and the photon modes and the direct coupling between the phonon and the magnon modes. In addition, a detailed discussion was directed regarding the numerical influences of the coupling strength between subsystems, the Kerr nonlinearity, and the effective detunings on the characteristics of the quantum coherence. The results help to achieve the nonreciprocal quantum coherence in a large parameter range, which has potential applications in achieving highly tunable information processing.

#### ACKNOWLEDGMENTS

This work is supported by the National Natural Science Foundation of China under Grants No. 12065008 and No. 12175199 and the Natural Science Foundation of Jiangxi Province under Grant No. 20224BAB201026.

- 
- [1] J. Li and S.-Y. Zhu, *New J. Phys.* **21**, 085001 (2019).
  - [2] Y.-P. Wang, G.-Q. Zhang, D. Zhang, T.-F. Li, C.-M. Hu, and J. Q. You, *Phys. Rev. Lett.* **120**, 057202 (2018).
  - [3] M. Goryachev, W. G. Farr, D. L. Creedon, Y. H. Fan, M. Kostylev, and M. E. Tobar, *Phys. Rev. Appl.* **2**, 054002 (2014).
  - [4] H. Huebl, C. W. Zollitsch, J. Lotze, F. Hocke, M. Greifenstein, A. Marx, R. Gross, and S. T. B. Goennenwein, *Phys. Rev. Lett.* **111**, 127003 (2013).
  - [5] Y. Tabuchi, S. Ishino, T. Ishikawa, R. Yamazaki, K. Usami, and Y. Nakamura, *Phys. Rev. Lett.* **113**, 083603 (2014).
  - [6] W. Zhang, D.-Y. Wang, C.-H. Bai, T. Wang, S. Zhang, and H.-F. Wang, *Opt. Express* **29**, 11773 (2021).
  - [7] V. Cherepanov, I. Kolokolov, and V. L'vov, *Phys. Rep.* **229**, 81 (1993).
  - [8] X. Zhang, C.-L. Zou, L. Jiang, and H. X. Tang, *Sci. Adv.* **2**, e1501286 (2016).
  - [9] J. Li, S.-Y. Zhu, and G. S. Agarwal, *Phys. Rev. Lett.* **121**, 203601 (2018).
  - [10] Y.-T. Chen, L. Du, Y. Zhang, and J.-H. Wu, *Phys. Rev. A* **103**, 053712 (2021).
  - [11] J. Li, S.-Y. Zhu, and G. S. Agarwal, *Phys. Rev. A* **99**, 021801(R) (2019).
  - [12] J. Zou, S. K. Kim, and Y. Tserkovnyak, *Phys. Rev. B* **101**, 014416 (2020).
  - [13] A. Kamra, E. Thingstad, G. Rastelli, R. A. Duine, A. Brataas, W. Belzig, and A. Sudbø, *Phys. Rev. B* **100**, 174407 (2019).
  - [14] H. Y. Yuan, P. Yan, S. S. Zheng, Q. Y. He, K. Xia, and M.-H. Yung, *Phys. Rev. Lett.* **124**, 053602 (2020).
  - [15] X. Y. Li, W.-X. Yang, T. Shui, L. Li, X. Wang, and Z. Wu, *J. Appl. Phys.* **128**, 233101 (2020).
  - [16] C. Kong, B. Wang, Z. X. Liu, H. Xiong, and Y. Wu, *Opt. Express* **27**, 5544 (2019).
  - [17] M. Aspelmeyer, T. J. Kippenberg, and F. Marquardt, *Rev. Mod. Phys.* **86**, 1391 (2014).
  - [18] B. Lenk, H. Ulrichs, F. Garbs, and M. Münzenberg, *Phys. Rep.* **507**, 107 (2011).
  - [19] A. A. Serga, A. V. Chumak, and B. Hillebrands, *J. Phys. D* **43**, 264002 (2010).
  - [20] G. Q. Zhang, Y. P. Wang, and J. Q. You, *Sci. China Phys. Mech. Astron.* **62**, 987511 (2019).
  - [21] Y.-P. Wang, G.-Q. Zhang, D. Zhang, X.-Q. Luo, W. Xiong, S.-P. Wang, T.-F. Li, C.-M. Hu, and J. Q. You, *Phys. Rev. B* **94**, 224410 (2016).
  - [22] Z.-X. Liu, B. Wang, H. Xiong, and Y. Wu, *Opt. Lett.* **43**, 3698 (2018).
  - [23] T. Baumgratz, M. Cramer, and M. B. Plenio, *Phys. Rev. Lett.* **113**, 140401 (2014).
  - [24] J. Xu, *Phys. Rev. A* **93**, 032111 (2016).
  - [25] A. Winter and D. Yang, *Phys. Rev. Lett.* **116**, 120404 (2016).
  - [26] H. Zhu, Z. Ma, Z. Cao, S. M. Fei, and V. Vedral, *Phys. Rev. A* **96**, 032316 (2017).
  - [27] A. Streltsov, U. Singh, H. S. Dhar, M. N. Bera, and G. Adesso, *Phys. Rev. Lett.* **115**, 020403 (2015).
  - [28] A. Streltsov, S. Rana, P. Boes, and J. Eisert, *Phys. Rev. Lett.* **119**, 140402 (2017).
  - [29] Z. Yan, X. Jia, C. Xie, and K. Peng, *Phys. Rev. A* **84**, 062304 (2011).
  - [30] X. Qi, T. Gao, and F. Yan, *J. Phys. A* **50**, 285301 (2017).
  - [31] A. Streltsov, G. Adesso, and M. B. Plenio, *Rev. Mod. Phys.* **89**, 041003 (2017).



- [32] M. A. Nielsen and I. Chuang, *Quantum Computation and Quantum Information* (Cambridge University, Cambridge, England, 2000).
- [33] A. P. Reed, K. H. Mayer, J. D. Teufel, L. D. Burkhardt, W. Pfaff, M. Reagor, L. Sletten, X. Ma, R. J. Schoelkopf, E. Knill, and K. W. Lehnert, *Nat. Phys.* **13**, 1163 (2017).
- [34] M. Aspelmeyer, P. Meystre, and K. Schwab, *Phys. Today* **65**, 29 (2012).
- [35] F. Marquardt and S. M. Girvin, *Physics* **2**, 40 (2009).
- [36] R. Demkowicz-Dobrzański and L. Maccone, *Phys. Rev. Lett.* **113**, 250801 (2014).
- [37] F. Levi and F. Mintert, *New J. Phys.* **16**, 033007 (2014).
- [38] M. B. Plenio and S. F. Huelga, *New J. Phys.* **10**, 113019 (2008).
- [39] P. Rebentrost, M. Mohseni, and A. Aspuru-Guzik, *J. Phys. Chem. B* **113**, 9942 (2009).
- [40] C.-M. Li, N. Lambert, Y.-N. Chen, G.-Y. Chen, and F. Nori, *Sci. Rep.* **2**, 885 (2012).
- [41] S. Lloyd, *J. Phys.: Conf. Ser.* **302**, 012037 (2011).
- [42] J. J. Chen, J. Cui, Y. R. Zhang, and H. Fan, *Phys. Rev. A* **94**, 022112 (2016).
- [43] S. Braun, M. Friesdorf, S. S. Hodgman, M. Schreiber, J. P. Ronzheimer, A. Riera, M. del Rey, I. Bloch, J. Eisert, and U. Schneider, *Proc. Natl. Acad. Sci. USA* **112**, 3641 (2015).
- [44] A. V. Shcherbakova, K. G. Fedorov, K. V. Shulga, V. V. Ryazanov, V. V. Bolginov, V. A. Oboznov, S. V. Egorov, V. O. Shkolnikov, M. J. Wolf, D. Beckmann, and A. V. Ustinov, *Supercond. Sci. Technol.* **28**, 025009 (2015).
- [45] F. Fröwis, B. Yadin, and N. Gisin, *Phys. Rev. A* **97**, 042103 (2018).
- [46] W. Xiong, Y. Qiu, L. A. Wu, and J. Q. You, *New J. Phys.* **20**, 043037 (2018).
- [47] L. L. Zhai and J.-L. Guo, *Physica A* **587**, 126523 (2022).
- [48] Q. Zheng, J. Xu, Y. Yao, and Y. Li, *Phys. Rev. A* **94**, 052314 (2016).
- [49] X. Y. Li, W. J. Nie, A. X. Chen, and Y. H. Lan, *Phys. Rev. A* **96**, 063819 (2017).
- [50] G. Y. Li, W. J. Nie, X. Y. Li, M. C. Li, A. X. Chen, and Y. H. Lan, *Sci. China Phys. Mech. Astron.* **62**, 100311 (2019).
- [51] J. P. Dowling and G. J. Milburn, *Philos. Trans. R. Soc. A* **361**, 1655 (2003).
- [52] N. Killoran, F. E. S. Steinhoff, and M. B. Plenio, *Phys. Rev. Lett.* **116**, 080402 (2016).
- [53] D. Vitali, S. Gigan, A. Ferreira, H. R. Böhm, P. Tombesi, A. Guerreiro, V. Vedral, A. Zeilinger, and M. Aspelmeyer, *Phys. Rev. Lett.* **98**, 030405 (2007).
- [54] R. Ghobadi, S. Kumar, B. Pepper, D. Bouwmeester, A. I. Lvovsky, and C. Simon, *Phys. Rev. Lett.* **112**, 080503 (2014).
- [55] H. L. Huang, A. K. Goswami, W. S. Bao, and P. K. Panigrahi, *Sci. China Phys. Mech. Astron.* **61**, 060311 (2018).
- [56] W. Vogel and J. Sperling, *Phys. Rev. A* **89**, 052302 (2014).
- [57] L. F. Buchmann and D. M. Stamper-Kurn, *Ann. Phys.* **527**, 156 (2015).
- [58] L. F. Buchmann, S. Schreppler, J. Kohler, N. Spethmann, and D. M. Stamper-Kurn, *Phys. Rev. Lett.* **117**, 030801 (2016).
- [59] E. Verhagen and A. Alù, *Nat. Phys.* **13**, 922 (2017).
- [60] D. L. Sounas and A. Alù, *Nat. Photon.* **11**, 774 (2017).
- [61] M. Hafezi and P. Rabl, *Opt. Express* **20**, 7672 (2012).
- [62] M. Terraneo, M. Peyrard, and G. Casati, *Phys. Rev. Lett.* **88**, 094302 (2002).
- [63] B. Liang, B. Yuan, and J.-C. Cheng, *Phys. Rev. Lett.* **103**, 104301 (2009).
- [64] L. Fan, J. Wang, L. T. Varghese, H. Shen, B. Niu, Y. Xuan, A. M. Weiner, and M. Qi, *Science* **335**, 447 (2012).
- [65] Z. Shen, Y.-L. Zhang, Y. Chen, C.-L. Zou, Y.-F. Xiao, X.-B. Zou, F.-W. Sun, G.-C. Guo, and C.-H. Dong, *Nature Photon* **10**, 657 (2016).
- [66] V. V. Konotop and V. Kuzmiak, *Phys. Rev. B* **66**, 235208 (2002).
- [67] C. Kong, H. Xiong, and Y. Wu, *Phys. Rev. Appl.* **12**, 034001 (2019).
- [68] R. Huang, A. Miranowicz, J.-Q. Liao, F. Nori, and H. Jing, *Phys. Rev. Lett.* **121**, 153601 (2018).
- [69] B. Li, R. Huang, X. Xu, A. Miranowicz, and H. Jing, *Photon. Res.* **7**, 630 (2019).
- [70] M.-A. Miri, F. Ruesink, E. Verhagen, and A. Alù, *Phys. Rev. Appl.* **7**, 064014 (2017).
- [71] F. D. M. Haldane and S. Raghu, *Phys. Rev. Lett.* **100**, 013904 (2008).
- [72] Y. Hadad and B. Z. Steinberg, *Phys. Rev. Lett.* **105**, 233904 (2010).
- [73] X.-W. Xu and Y. Li, *Phys. Rev. A* **91**, 053854 (2015).
- [74] K. Szulc, P. Graczyk, M. Mruczkiewicz, G. Gubbiotti, and M. Krawczyk, *Phys. Rev. Appl.* **14**, 034063 (2020).
- [75] J. Lan, W. Yu, R. Wu, and J. Xiao, *Phys. Rev. X* **5**, 041049 (2015).
- [76] J. Zou, S. Bosco, E. Thingstad, J. Klinovaja, and D. Loss, *arXiv:2306.15916*.
- [77] K. Xia, F. Nori, and M. Xiao, *Phys. Rev. Lett.* **121**, 203602 (2018).
- [78] D. Malz, L. D. Tóth, N. R. Bernier, A. K. Feofanov, T. J. Kippenberg, and A. Nunnenkamp, *Phys. Rev. Lett.* **120**, 023601 (2018).
- [79] Z. Shen, Y.-L. Zhang, Y. Chen, F.-W. Sun, X.-B. Zou, G.-C. Guo, C.-L. Zou, and C.-H. Dong, *Nat. Commun.* **9**, 1797 (2018).
- [80] S. Barzanjeh, M. Wulf, M. Peruzzo, M. Kalaei, P. B. Dieterle, O. Painter, and J. M. Fink, *Nat. Commun.* **8**, 953 (2017).
- [81] S. Maayani, R. Dahan, Y. Kligerman, E. Moses, A. U. Hassan, H. Jing, F. Nori, D. N. Christodoulides, and T. Carmon, *Nature (London)* **558**, 569 (2018).
- [82] Z.-B. Yang, J.-S. Liu, A.-D. Zhu, H.-Y. Liu, and R.-C. Yang, *Ann. Phys. (Leipzig)* **532**, 2000196 (2020).
- [83] Y.-F. Jiao, S.-D. Zhang, Y.-L. Zhang, A. Miranowicz, L.-M. Kuang, and H. Jing, *Phys. Rev. Lett.* **125**, 143605 (2020).
- [84] Q. Zheng, W. Zhong, G. Cheng, and A. Chen, *Opt. Commun.* **546**, 129796 (2023).
- [85] Y. Xu, J.-Y. Liu, W. Liu, and Y.-F. Xiao, *Phys. Rev. A* **103**, 053501 (2021).
- [86] X. Zhang, C.-L. Zou, L. Jiang, and H. X. Tang, *Phys. Rev. Lett.* **113**, 156401 (2014).
- [87] C. Genes, A. Mari, P. Tombesi, and D. Vitali, *Phys. Rev. A* **78**, 032316 (2008).
- [88] S. Cheng and M. J. W. Hall, *Phys. Rev. A* **92**, 042101 (2015).
- [89] A. Hertz, E. Karpov, A. Mandilara, and N. J. Cerf, *Phys. Rev. A* **93**, 032330 (2016).
- [90] D. Miki, A. Matsumura, and K. Yamamoto, *Phys. Rev. D* **105**, 026011 (2022).